Tryptophol acetate and tyrosol acetate, metabolites secreted by a probiotic yeast, block cytokine storm

Orit Malka[1†], Ravit Malishev[1†], Marina Bersudsky[2], Manikandan Rajendran[1], Mathumathi Krishnamohan[2], Jakeer Shaik[2], Daniel Chamovitz[1], Evgeni Tikhonov[3], Eliya Sultan[2,4], Omry Koren[3], Ron N. Apte[2], Benyamin Rosental[2,4], Elena Voronov[2*], Raz Jelinek[1,5*].

*Correspondence: elena@bgu.ac.il; razj@bgu.ac.il

[1] Department of Chemistry, Ben-Gurion University of the Negev, 84105 Be'er Sheva, Israel

[2] Department of Microbiology and Immunology, Faculty of Health Sciences, The Cancer Research Center, Ben-Gurion University of the Negev, Beer-Sheva 84105, Israel

[3] The Azrieli Faculty of Medicine, Bar Ilan University, 1311502 Safed, Israel

[4] Regenerative Medicine and Stem Cell Research Center, Ben-Gurion University of the Negev.

[5] Ilse Katz Institute for Nanoscale Science & Technology Ben Gurion University of the Negev, Be'er Sheva 84105, Israel;

† These authors contributed equally to this work

Abstract

Probiotic fermented foods are perceived as contributing to human health and capable of protecting against inflammation processes, however solid mechanistic evidence for the putative therapeutic benefits are generally lacking. Here we report that tryptophol acetate and tyrosol acetate, small molecule metabolites secreted by the probiotic milk-fermented yeast *Kluyveromyces marxianus* exhibit remarkable anti-inflammatory properties. Comprehensive *in vivo* and *in vitro* experimental analyses, employing LPS-induced "cytokine storm" models, reveal dramatic effects of the two molecules, added in tandem, on mice morbidity, laboratory parameters and mortality. In parallel, significant attenuation of pro-inflammatory cytokines including IL-6, IL-1α, IL-1β and TNF-α, and reduction of reactive oxygen species were recorded. Importantly, tryptophol acetate and tyrosol acetate did not completely suppress cytokine generation, but rather brought their concentrations back to baseline levels, enabling maintenance of core immune functions, including phagocytosis. The anti-inflammatory effects of tryptophol acetate and tyrosol acetate were mediated through downregulation of TLR4, IL-1R, and TNFR signaling pathways and increased A20 expression, leading to NF-kB attenuation. Moreover, the two molecules had a significant impact on mice microbiome, increasing the abundance of the genus *Bactericides,* known to exhibit anti-inflammatory properties. Overall, this work illuminates pronounced and broad-based immune modulation properties of probiotic yeast-secreted metabolites, underscoring potential new therapeutic avenues for severe inflammation pathologies.

Importance

Probiotic fermented foods are perceived as contributing to human health and capable of protecting against inflammation, however biological/molecular evidence for the presumptive health benefits are generally lacking. This paper reports the identification of two small molecule metabolites secreted by milk-fermented probiotic yeast, shown to exert remarkable anti-inflammatory effects. In particular, the small molecules - tryptophol acetate and tyrosol acetate – block severe inflammation, commonly known as "cytokine storm", in cell and mice models. Importantly, tryptophol acetate and tyrosol acetate did not completely suppress immune response, but rather brought the immune system back to baseline levels, enabling maintenance of its protective functions. The anti-inflammatory mechanisms of tryptophol acetate and tyrosol acetate were deciphered, shedding light on the immune modulation properties of probiotic yeast. This study underscores a molecular basis for the therapeutic potential of milk-fermented probiotics, and charts new avenues for treatment of severe inflammation.

Introduction

Sepsis is a life-threatening condition manifested by severe inflammation leading to multiple organ dysfunction. The inflammatory host response associated with both innate and adaptive immunity mechanisms play an important role in the development of the clinical and pathological manifestations of sepsis[1]. Recently, it has been found that the prognosis of the disease is dependent not only on the virulence of the microorganisms, but, mainly, on the host response affected by the pathogen-associated molecular patterns (PAMPs) [2,3]. Recruitment of immune cells and secretion of soluble mediators by the cells can exacerbate the severity of the disease [4]. Specifically, the

release of pro-inflammatory molecules, such as interleukin-6 (IL-6), tumor necrosis factor-alpha (TNF-α) and interleukin-1α and 1β (IL-1α and IL-1β), trigger "cytokine storms", systemic inflammation often leading to multi-organ failure and adverse clinical outcomes with high mortality rates [5]. Cytokine storms occur in various disease conditions, including sepsis and septic shock [6] and acute stages in chronic diseases [7]. Severe inflammation and the occurrence of cytokine storms were also shown to be major causes of mortality from COVID-19 [8,9].

Despite the significant progress in inflammation treatment following the discovery of antibiotics, high mortality from sepsis still exists. Thus, new approaches to improve conventional therapies are highly sought. Varied food products have been touted to endow anti-inflammatory properties and as such attract significant interest [10]. Food-extracted substances have been particularly explored as anti-inflammatory agents, including probiotics [11,12], curcumin [13], resveratrol [14], plant extracts [15], and phenolic compounds from natural sources [16]. However, the therapeutic benefits of most such substances against severe inflammation have been limited [17], and, moreover, detailed mechanistic understanding of their perceived anti-inflammatory properties are generally lacking.

Probiotics, particularly milk-fermented microorganism mixtures (yogurt, kefir), have been known to bolster the innate immune system and host-defense mechanisms against pathogens [18,19]. In a recent study, we reported on a yet-unrecognized mechanism for cross-kingdom inhibition of pathogenic bacterial communication and virulence by a small molecule - tryptophol acetate – secreted by the probiotic yeast *Kluyveromyces marxianus* in a milk-fermented probiotic microorganism mixture [20]. Specifically, tryptophol acetate was found to disrupt biofilm formation and reduce virulence of

several human pathogenic bacteria, underscoring a novel mechanism for combating bacterial colonization and pathogenicity.

Here, we report that tryptophol acetate and tyrosol acetate, another *K. marxianus* – secreted metabolite, exhibit remarkable anti-inflammation activities, in *in vitro, ex vivo* and *in vivo* models. Through application of LPS-induced cytokine storm, we observed that the two molecules had anti-oxidation, anti-inflammatory, clinical, histological and hematological systemic protective effects against severe inflammation. Importantly, tryptophol acetate and tyrosol acetate did not give rise to immune system shutdown, rather reduced pro-inflammatory cytokine production to baseline levels while retaining core immune processes including phagocytosis and generation of anti-inflammatory cytokines. Detailed molecular analysis indicates that the anti-inflammatory activities of tryptophol acetate and tyrosol acetate are mediated through downregulation of *TLR4*, *IL-1R*, and *TNFR* signaling pathways and suppression of NF-κB activity. In particular, we discovered that the molecules enhanced expression of A20, a key modulator of NF-κB signaling pathways [21]. Overall, this study demonstrates remarkable anti-inflammatory properties of probiotic yeast-secreted metabolites and furnishes a detailed mechanistic description of the effects, underscoring their significant therapeutic potential.

Results and Discussion

Anti-oxidation properties of tryptophol acetate and tyrosol acetate

Scheme 1 depicts the chemical structures of tryptophol acetate (**1**) and tyrosol acetate (**2**), recently identified as metabolites secreted by the probiotic fungus *Kluyveromyces marxianus* in milk-fermented microorganism mixture ("kefir"), and shown to exhibit

intriguing antibacterial properties through blocking quorum sensing [22]. Importantly, no inflammation-modulatory activities have been previously reported for neither tryptophol acetate nor tyrosol acetate.

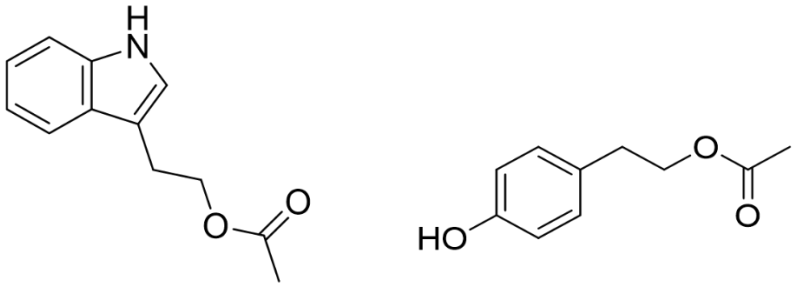

Tryptophol acetate **(1)** Tyrosol acetate **(2)**

Scheme 1. Chemical structures of tryptophol acetate (1) and tyrosol acetate (2).

We first analyzed the anti-oxidation properties of the molecules (Figure 1) as oxidation processes and generation of reactive oxidative species (ROS) are recognized as contributing to toxic effects in diverse diseases and pathological conditions [23]. Figure 1 depicts application of a spectrophotometric assay monitoring the visible absorbance of the 2,2-diphenyl-1-picrylhydrazyl (DPPH) radical, which is widely employed for evaluating the anti-oxidation activity of biomolecules [24]. In this assay, the DPPH free radical, stable at room temperature, is reduced in the presence of an antioxidant molecule, giving rise to a colorless ethanol solution. The bar diagram in Figure 1A shows the degree of quenching of DPPH radical absorbance (and concomitant anti-oxidative properties) by tryptophol acetate and tyrosol acetate, when added individually as well as together, resembling their presence in the kefir. Figure 1A indicates a dramatic anti-oxidation effect for the mixture of the two molecules**.** Specifically, while **1** individually gave rise to 10% quenching of DPPH absorbance and **2** alone reduced

the absorbance by ~3%, when the **1** and **2** were added together (at the same concentrations) to the DPPH solution, 30% absorbance attenuation was recorded (Figure 1A).

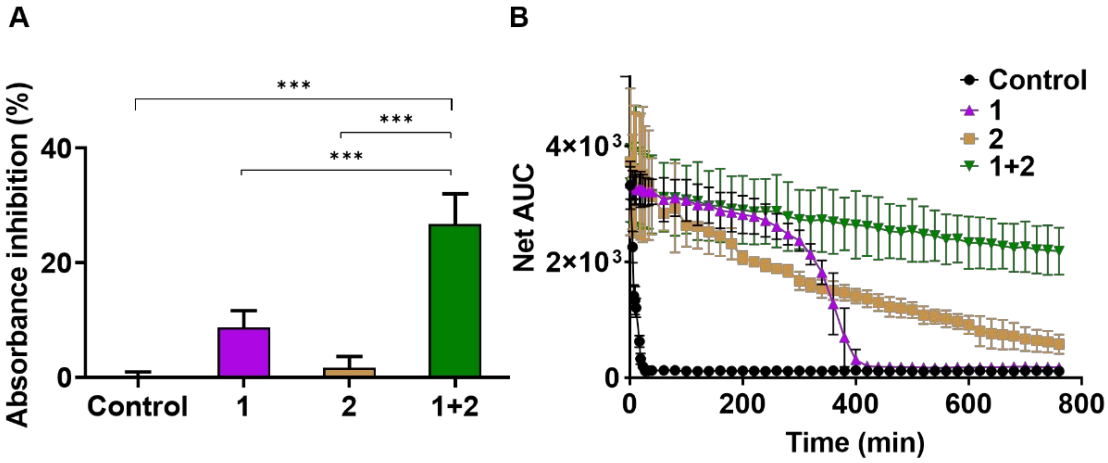

Figure 1. Anti-oxidation effect of tryptophol acetate and tyrosol acetate. Anti-oxidative capacity of the molecules as measured by DPPH (**A**) and ORAC (**B**) assays. **A.** The results are presented as a percentage of absorbance inhibition (517 nm, the absorbance maximum of DPPH) in the presence of tryptophol acetate (**1**) alone, tyrosol acetate alone (**2**) alone, and **1**+**2** together. **B**. Fluorescence decay of fluorescein induced by AAPH in the absence or presence of **1** and **2**. Reaction mixtures containing fluorescein (60 nM) and AAPH (18.75 mM) in 200 µl of phosphate buffer (75 mM, pH 7.4) were incubated at 37°C for 800 min. Changes in fluorescence intensity emitted by fluorescein were monitored. Results are presented as the net area under the curve (AUC). Each value is the mean ± SD of triplicate experiments. ***p<0.0001

The results of the oxygen radical absorbance capacity (ORAC) assay in Figure 1B further demonstrate substantial anti-oxidation activity by tryptophol acetate and tyrosol acetate when added together. The ORAC experiment measures the quenching of fluorescein emission by peroxyl radicals, and inhibition of the oxidation reaction by molecular species added to the solution [25]. As shown in Figure 1B, in the control sample, the fluorescence emission recorded for fluorescein decreased instantaneously because of the significant quenching induced by the peroxyl radicals. However, upon co-addition of **1** or **2**, the fluorescence decays were significantly longer, up to around

400 min (in the case of **1,** purple curve) and 800 min (for **2**, beige curve), likely accounting for scavenging of the peroxyl radical by the molecules. Strikingly, significant inhibition of peroxyl-induced fluorescence quenching occurred when tryptophol acetate and tyrosol acetate were added together to the solution (green curve in Figure 1B), underscoring their anti-oxidation effect according to their existence in the kefir.

Oral uptake of tryptophol acetate and tyrosol acetate mixture provides protection against LPS-induced cytokine storm in mice

As tryptophol acetate and tyrosol acetate exhibit more powerful anti-oxidation activity as a mixture , we next investigated the anti-inflammatory properties of the **1+2** mixture *in vivo* using a model of lipopolysaccharide (LPS)-induced inflammation, which triggers a massive pro-inflammatory cytokine release identified as a "cytokine storm" [26,27]. In the experiments, C57BL/6 mice were injected with LPS (30 mg/kg), and the effects of the **1** + **2** mixture administrated orally by gavage (each molecule at 150 µg/Kg per mouse) were monitored up to 156 hours after LPS injection (scheme in Figure 2A).

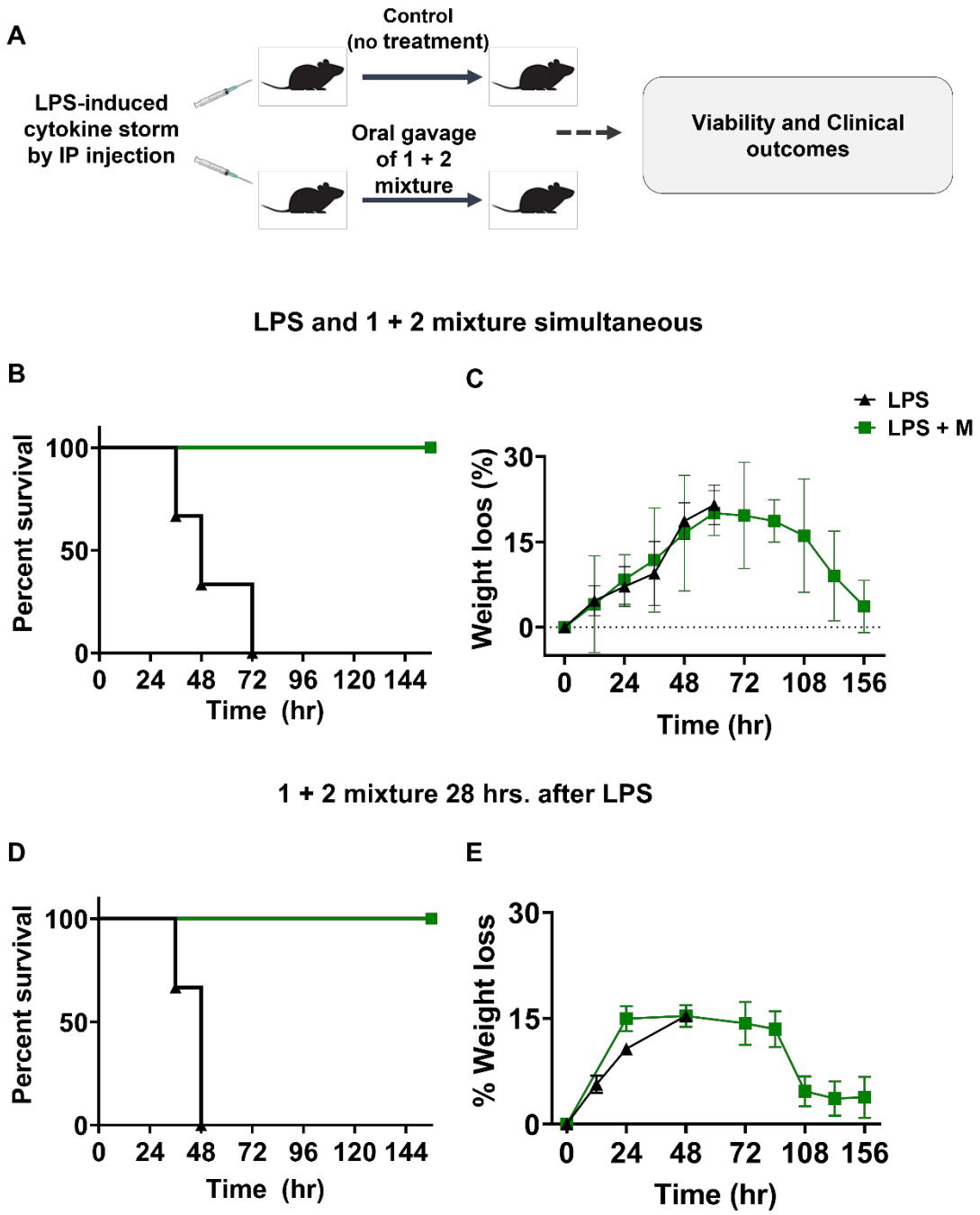

Figure 2. Tryptophol acetate and tyrosol acetate mixture shield mice from LPS-induced severe inflammation. (**A**) Experimental scheme. After intraperitoneal (IP) injection of LPS (30 mg/kg), mice were randomly divided into two groups, PBS-treated and treated with **1**+**2** immediately after LPS injection (**B, C**). A third group treated with the molecules 28 hours after LPS injection (**D, E**). Survival (**B, D**) and weight loss (**C, E**) of the mice were monitored for 156 hours .(n=6 in each group)

Initially, mice were injected with LPS and at the same time interval were treated with **1+2** mixture. The percentage survival and weight loss in the LPS-administered mice, with and without treatment, show that the molecules mixture significantly improved the disease outcome. Remarkably, while all LPS-treated mice died within 72 hours due to the severe inflammation (i.e. the "cytokine storm"), 100% of the mice orally given the mixture of **1** + **2** survived (Figure 2B). Furthermore, the LPS-administered mice experienced substantial weight loss prior to mortality (Figure 2C, black line). In contrast, mice which were orally treated with the molecular mixture, initially lost weight (up to 60 hours), but reverted to their initial values within 156 hours (Figure 2C, green line).

To prove the therapeutic effects of the molecules, we carried out another experiments, in which **1+2** mixture was given to mice that were already impacted by the onset of LPS-induced inflammation (Figure 2D-E). In these experiments, the molecular mixture was administered to the mice by gavage 28 hours after LPS injection. At this time-interval, severe signs of the disease were already evident, including decreased motor activities, ruffled fur, diarrhea, substantial eye discharge and respiratory distress. Notably, the results in Figure 2D demonstrate that while all untreated mice died within 48 hours after LPS injection, 100% of the mice treated with the **1** + **2** mixture survived. The weight lost patterns in mice treated with the molecules 28 hours after LPS administration when severe inflammation was already developed (Figure 2E) were similar to the case of mice that were orally given the two molecules simultaneously with LPS (e.g., Figure 2C). Overall, the results presented in Figure 2 demonstrate an exceptional therapeutic effect of the tryptophol acetate and tyrosol acetate mixture.

Oral uptake of tryptophol acetate and tyrosol acetate decreased tissue damage induced by LPS

Cytokine storms generally account for multisystem failure manifested in considerable damage to the lungs, liver, and the gastrointestinal (GI) tract [28]. To investigate whether the healing effects of tryptophol acetate and tyrosol acetate (e.g., Figure 2) also lead to reduced organ damage, we carried out histology analyses of different tissues obtained from LPS-injected mice treated or non-treated with the **1+2** mixture (Figure 3). The representative hematoxylin and eosin (H&E) staining image of lung tissue from a healthy mouse displays normal alveolar walls and no inflammatory cell infiltration (Figure 3A, top row). In LPS-injected mice, signs of severe lung injury characterized by lung edema, hemorrhage, intensive cellular infiltrate, and accumulation of fibrin were observed already during the first 6 hours (Figure 3A, middle panel).

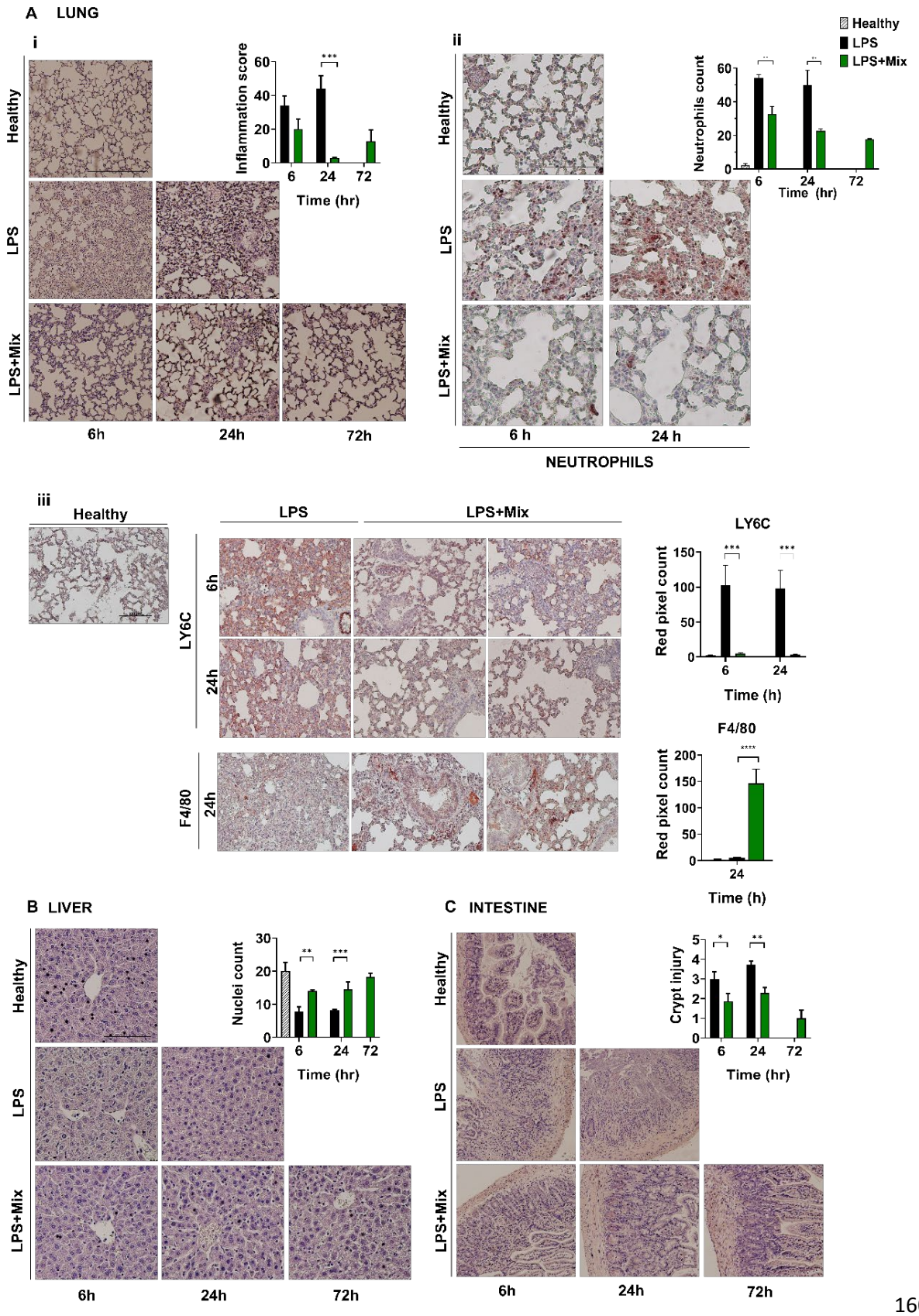

Figure 3. Tryptophol acetate and tyrosol acetate prevent inflammation-associated tissue damage. A(i), B and C Representative pictures of H&E-stained sections of

obtained organs from healthy and LPS-injected mice with or without administration of molecule mixture (**A(i)**) lung, (**B**) liver and (**C**) small intestine samples. Original magnification x20 for lung and small intestine, x10 for liver. Quantification of tissue damage was performed, as discussed in Materials and Methods (M&M) and is presented as a bar diagram on top of each panel. **(A (ii))** Lung tissues obtained 6 and 24 h after LPS administration were stained with anti-myeloperoxidase (MPO) antibodies for neutrophils detection. Original magnification x10. of the ammount of neutrophils was counts as discribed in M&M and presented in the graph. **(A(iii))** Monocytes were detected by anti-Ly6C antibodies and macrophages by anti-F4/80 antibodies. Quantification of the positive cells was assessed, as described. Insert in panel B represents an amount of hepatocytes with preserved cell structure. Insert in panel C represents quantification of intestinal crypt damage. Representative pictures are presented in magnification x20. *p < 0.05; **p < 0.01; ***p < 0.0001 ****p<0.00001

Strikingly, lung tissue damage was largely eliminated in mice to which the **1+2** mixture was co-administered with LPS [Figure 3A(i), bottom row]. Indeed, the pulmonary architecture was mostly preserved in those mice, with only small local zones of inflammation. In addition, the alveolar walls were almost not altered, and minimal accumulation of inflammatory cells was observed at the indicated time intervals. Notably, after 72 hours (in which only mice treated with the molecules survived), the lung structure was similar to the structure observed in healthy mice (Figure 3A(i)). Lung tissue damage was assessed by quantification of pathological score [bar diagram in Figure 3A(i), inset]. Indeed, the increase in mean pathological score after LPS administration, was significantly reduced after treatment with **1** + **2** mixture (at 24 and 72 hours). Those findings demonstrate that tryptophol acetate and tyrosol acetate mixture effectively blocked inflammation-induced damage in lungs.

To further examine the protective effects of the molecules on lung damage after LPS-induced inflammation, we assessed the recruitment of myeloid cells into the lungs (Figure 3A,ii-iii). In the experiments, we performed immunohistochemical (IHC) staining with anti-MPO antibodies for neutrophils, anti-Ly6C antibodies for monocytes

(Ly6C^{positive}) and anti-F4/80 antibodies for macrophages (F4/80^{pos}), considered mature macrophages [29]. Figure 3A(ii), top row, shows minimal neutrophil infiltration in lungs from control mice**.** However, lungs of LPS-treated mice displayed significant recruitment of neutrophils already 6 hours after LPS injection (Figure 3A(ii), middle row). Remarkably, in mice which received the **1**+**2** mixture, the recruitment of neutrophils was significantly decreased and was comparable to healthy (PBS treated) mice (bar diagram in Figure 3A(ii), inset).

Figure 3A(iii) illuminates the recruitment of monocytes and macrophages into the lungs. Both types of cells are strongly associated with inflammation-induced lung pathogenesis [30,31]. Lung-recruited Ly6C^{pos} monocytes account for microvascular endothelial cell activation and vascular injury in LPS-induced early endotoxemia, leading to enhanced pulmonary vascular leakage [32,33]. Figure 3A,iii shows that while the abundance of lung-recruited Ly6C^{pos} monocytes significantly increased following LPS administration both after 6 and 24 hours, treatment with tryptophol acetate and tyrosol acetate mixture effectively reduced Ly6C^{pos} monocytes levels back to baseline (i.e. healthy mice). In contrast, treating mice with **1+2** mixture increased F4/80^{pos} myeloid cells (Figure 3A,iii, bottom row), as these macrophages are associated with suppression of inflammation in lung tissues [29,34].

Figure 3B indicates that **1+2** mixture also prevented tissue damage in the liver. The H&E staining image of healthy liver is presented in Figure 3B, top row. In contrast, the structure of liver tissue was significantly damaged 6 and 24 hours after LPS administration, in which acute inflammatory response was apparent, characterized by decreased cell density, enlarged cell gaps and neutrophil infiltration. Morphological changes in the liver tissue, however, were markedly decreased in mice treated with **1+2** mixture (Figure 3B, bottom panels). Indeed, administration of **1** and **2** featured higher

number of normal nuclear cells in comparison to LPS-administered mice that were untreated with the molecules (bar diagram in Figure 3B, inset).

Similar prevention of tissue damage by tryptophol acetate and tyrosol acetate was apparent in the small intestine (Figure 3C). Specifically, H&E staining of intestinal tissues extracted from LPS-injected mice displayed an extensive damage of both mucosa and sub-mucosa, loss of intestinal mucosal crypt morphology and recruitment of inflammatory cells (Figure 3C, middle row). In comparison, mice treated with **1** + **2** mixture exhibited markedly lower tissue damage (Figure 3C, bottom row). Quantification of crypt injury (Figure 3C, inset) attests to the significantly lower tissue damage, in all time points, in LPS-injected mice treated with the two molecules.

Effects of oral uptake of tryptophol acetate and tyrosol acetate on systemic inflammation.

We further assessed the effects of the tryptophol acetate and tyrosol acetate mixture oral uptake on systemic inflammation (Figure 4). In the experiments depicted in Figure 4, the peripheral cell blood count (CBC) was evaluated at different time intervals. The results show that in LPS-injected mice that were not treated with **1+2,** significant reductions in red blood cell (RBC) counts, hemoglobin (HGB) and hematocrits (HCT) occurred. Notably, however, addition of **1** + **2** mixture significantly increased these parameters (Figure 4A top row, green lines vs black lines). Treating mice with **1** + **2** mixture also increased thrombocyte counts (PLT), which were reduced after LPS injection (Figure 4A). The CBC data in Figure 4A indicate that tryptophol acetate and tyrosol acetate prevented both inflammation-induced anemia and thrombocytopenia that are usually associated with severe inflammation, especially accompanied by

cytokine storms [35]. Notably, Figure 4A further reveals insignificant cell count changes in the white blood cells (WBC) and granulocytes (GRA).

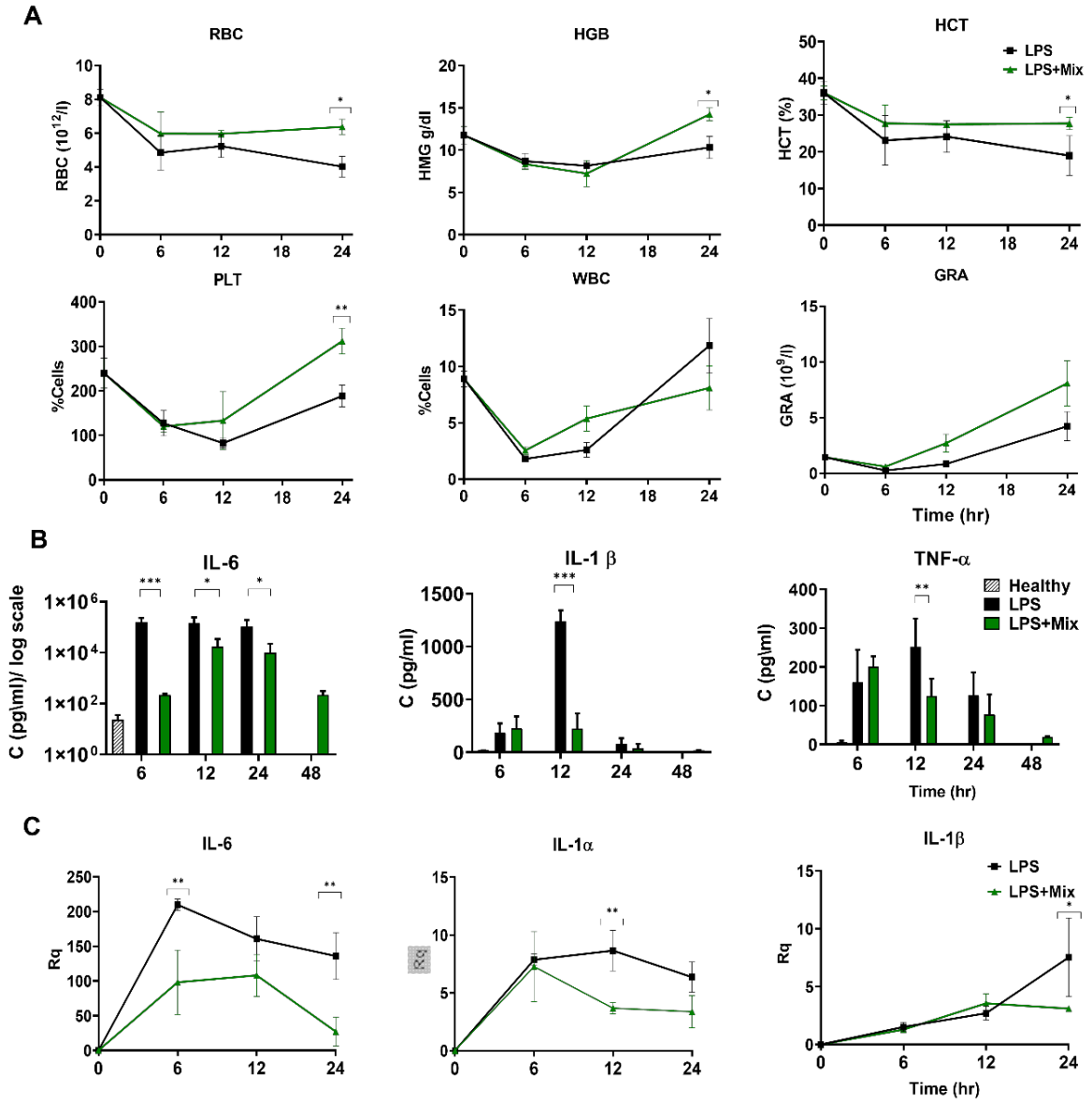

Figure 4. Effects of tryptophol acetate and tyrosol acetate mixture on systemic inflammation. Samples of the peripheral blood were obtained from the tail vein at different time intervals and assessed for CBC. Serums were collected and studied by ELISAs. **A**. The results of RBC, HGB, HCT, PLT, WBC, GRA at different time intervals. LPS-administered mice with PBS treatment (black lines) and treated with **1**+**2 mixture** (green), *p < 0.05. **B.** Cytokine levels in serum, assessed by commercial ELISA kits. Data are presented as mean ± SD in each group (n=3). *p<0.05l, **p<0.005, ***p<0.0001. **(C)** Lungs were obtained from LPS treated mice at indicated time intervals and mRNA was extracted and proceed to RTPCR. Expression of IL-6, IL-1α and IL-1β is shown. Data are shown as mean ± SD in each group (n=4). *p<0.05, **p<0.005.

The clinical hallmark of cytokine storms is the increased secretion of pro-inflammatory cytokines. Accordingly, we determined the effects of tryptophol acetate and tyrosol acetate mixture given orally to the LPS-injected mice on the levels of pro-inflammatory cytokines, including IL-6, IL-1β and TNF-α in serums (Figure 4B) and lungs (Figure 4C). Figure 4B demonstrates that while LPS injection increased the levels of cytokines in serum, treatment with **1**+**2** mixture significantly attenuated cytokine concentrations within 6-24 hours (Figure 4B). Specifically, blood concentrations of IL-6 in LPS-administered mice treated with the molecules were lower compared to the untreated LPS-injected mice in all time intervals (note that after 48 hours, LPS-administered mice treated with PBS did not survive, Figure 4B). However, after 48 hours, the IL-6 level of treated mice was almost identical to the healthy mice. Statistically significant reductions of IL-1β and TNF-α levels in LPS-administered mice that received the **1**+**2** mixture was observed 12 hours after LPS injection (Figure 4B).

Tryptophol acetate and tyrosol acetate mixture also inhibited the expression of pro-inflammatory cytokines in the lungs (Figure 4C). Specifically, while LPS administration significantly elevated the mRNA levels of IL-6, IL-1α, and IL-1β in lung tissues, oral treatment with **1** + **2** mixture reduced the expression of these cytokines at the examined time intervals (Figure 4C). Thus, oral administration of tryptophol acetate and tyrosol acetate mixture decreased cytokine secretion in serum (Figure 4B) and expression (Figure 4C) thereby inhibiting severe systemic inflammation after LPS injection.

Tryptophol acetate and tyrosol acetate reduced the production of ROS and pro-inflammatory cytokines in LPS-activated murine peritoneal macrophages, without reducing phagocytosis function

To investigate the mechanistic basis of the clinical and biological immunomodulation effects of tryptophol acetate and tyrosol acetate (e.g., Figures 1-4), we performed *ex-vivo* experiments using murine peritoneal macrophages. Figure 5A depicts the effects of tryptophol acetate and tyrosol acetate on reactive oxygen species (ROS) generation using the CellRox Deep-Red dye assay. In general, elevated inflammation levels go together with enhanced production of ROS [36]. Oxidative stress conditions were attained in the experiments by stimulating the murine peritoneal macrophages with LPS (100 ng/ml) with or without co-addition of the **1**+**2** mixture. The flow cytometry analysis revealed a significant decrease in intracellular ROS after 16 hours incubation of LPS-stimulated macrophages with **1** + **2** mixture**,** in comparison with the untreated LPS-stimulated macrophages (Figure 5A).

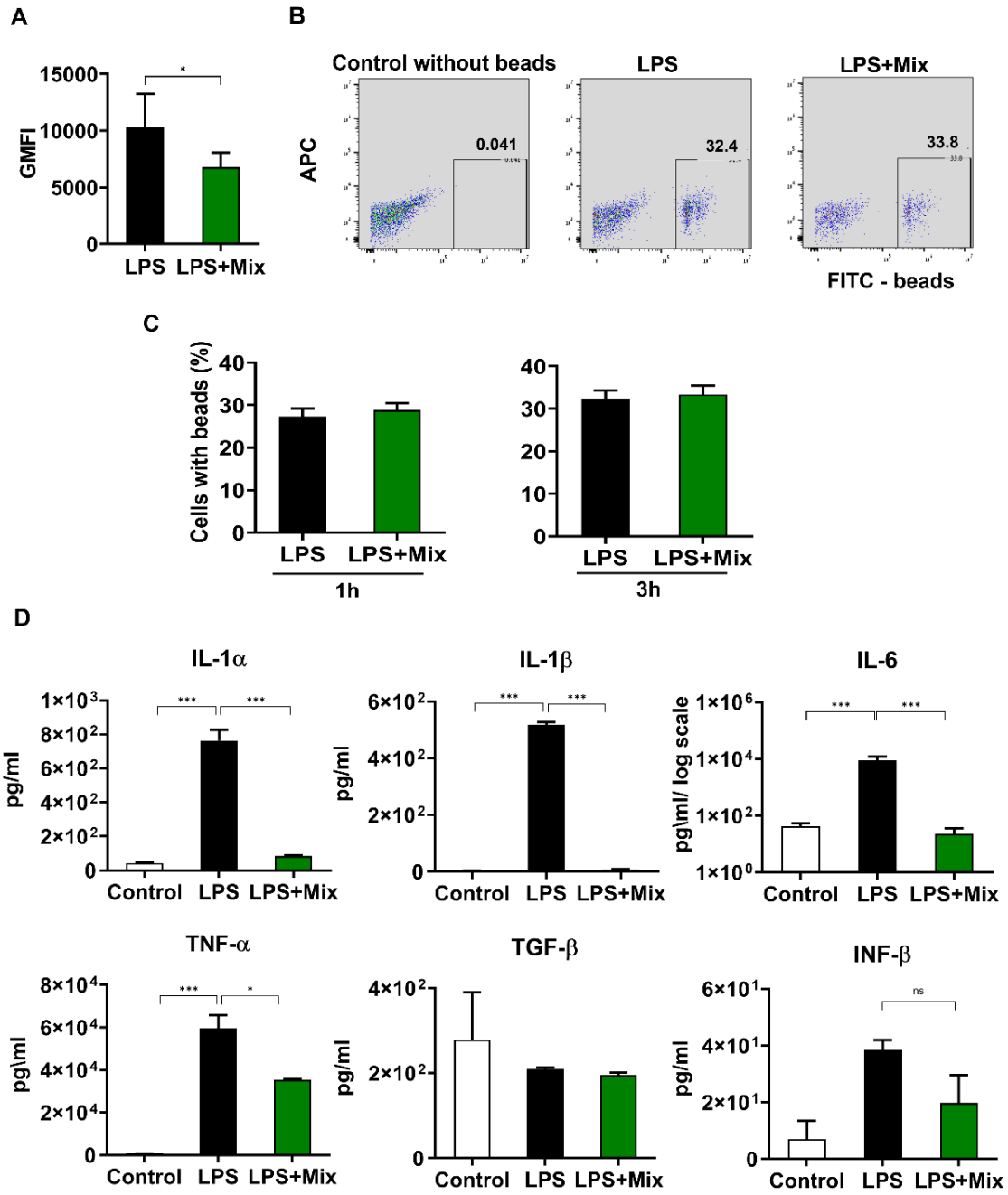

Figure 5. Anti-inflammatory properties of tryptophol acetate and tyrosol acetate *ex vivo*. A. Intracellular reactive oxygen species (ROS) after LPS stimulation of murine peritoneal macrophages (three replicates flow cytometry analysis), the results are the Geometric Mean Fluorescent Intensity (GMFI) of the CellRox Deep-Red dye. (Unpaired t-test, $p<0.05$; n=14). **B**. Representative scatter plots and gating conditions for green-fluorescent beads engulfment analysis, depicting bead uptake after 1 hour incubation of the macrophages, with or without co-addition of **1**+**2** mixture. Percentages of bead positive cells are indicated in the bottom right quadrants. **C**. Analysis of phagocytosis function of murine peritoneal macrophages after LPS stimulation incubated for 1 or 3 hours with or without molecules in concentration of 100 μM each by using green-fluorescent beads (Unpaired t-test, two-tailed; $p<0.05$). **D**.

Cytokine levels determined by ELISA from supernatants of *ex-vivo* isolated peritoneal murine macrophages. Macrophages were incubated for 16-hour with and without LPS and **1**+**2** mixture. Results presented as mean ± SD; n=3 from two independent experiments. *p<0.05 ***p<0.0001.

Since phagocytosis is a key function of macrophages [37], we examined macrophage phagocytic action in LPS-stimulated murine peritoneal macrophages with and without co-incubation with the **1** + **2** mixture (Figure 5B,C). Phagocytosis was assessed in the experiments by flow cytometry measuring the uptake of green-fluorescent beads by the cells. The representative gating analysis by flow cytometry (1 hour phagocytosis assay, Figure 5B) together with the bar diagram (Figure 5C) demonstrate no difference in the phagocytic activity of LPS-stimulated macrophages in the absence or presence of the **1**+**2** mixture (1 and 3 hours of phagocytosis assays). These results indicate that the tryptophol acetate and tyrosol acetate mixture did not adversely affect the phagocytic ability of macrophages.

To further confirm the immunomodulatory effects of tryptophol acetate and tyrosol acetate *ex vivo*, we quantified production of pro-inflammatory cytokines by the LPS-stimulated murine peritoneal macrophages with and without co-incubation with the molecule mixture (Figure 5D). Indeed, while the production of IL-1α, IL-1β, IL-6, and TNF-α by macrophages increased within 16 hours after LPS stimulation, addition of the **1**+**2** mixture significantly reduced the concentrations of all these pro-inflammatory cytokines, in most cases back to the non-stimulated macrophage levels. In contrast, tryptophol acetate and tyrosol acetate did not affect secretion of the anti-inflammatory cytokines TGF-β and INF-β (Figure 5D). These results again demonstrate that the addition of the molecule mixture did not disrupt core anti-inflammatory mechanisms of the host. Together, the results presented in Figure 5 demonstrate that tryptophol acetate

and tyrosol acetate decreased intracellular ROS and inhibited generation of pro-inflammatory cytokines, while not adversely affecting important immune processes, including macrophage phagocytic function and anti-inflammatory cytokine production.

Effect of tryptophol acetate and tyrosol acetate on NF-κB pathways in LPS-activated macrophages ex vivo and in vitro

To obtain further insight into the molecular contours underlining the immune modulating activities of the tryptophol acetate and tyrosol acetate mixture, we investigated intracellular pathways associated with NF-κB, a key protein in major inflammation gene cascades [38] (Figure 6). Indeed, the representative western blot (WB) image in Figure 6A (**i**) demonstrates that addition of **1** + **2** mixture to the LPS-stimulated macrophages markedly inhibited generation of the phosphorylated form of NF-κB (p65) in comparison to stimulation with LPS (relative band intensities are depicted in the bar diagram in Figure 6A (ii)).

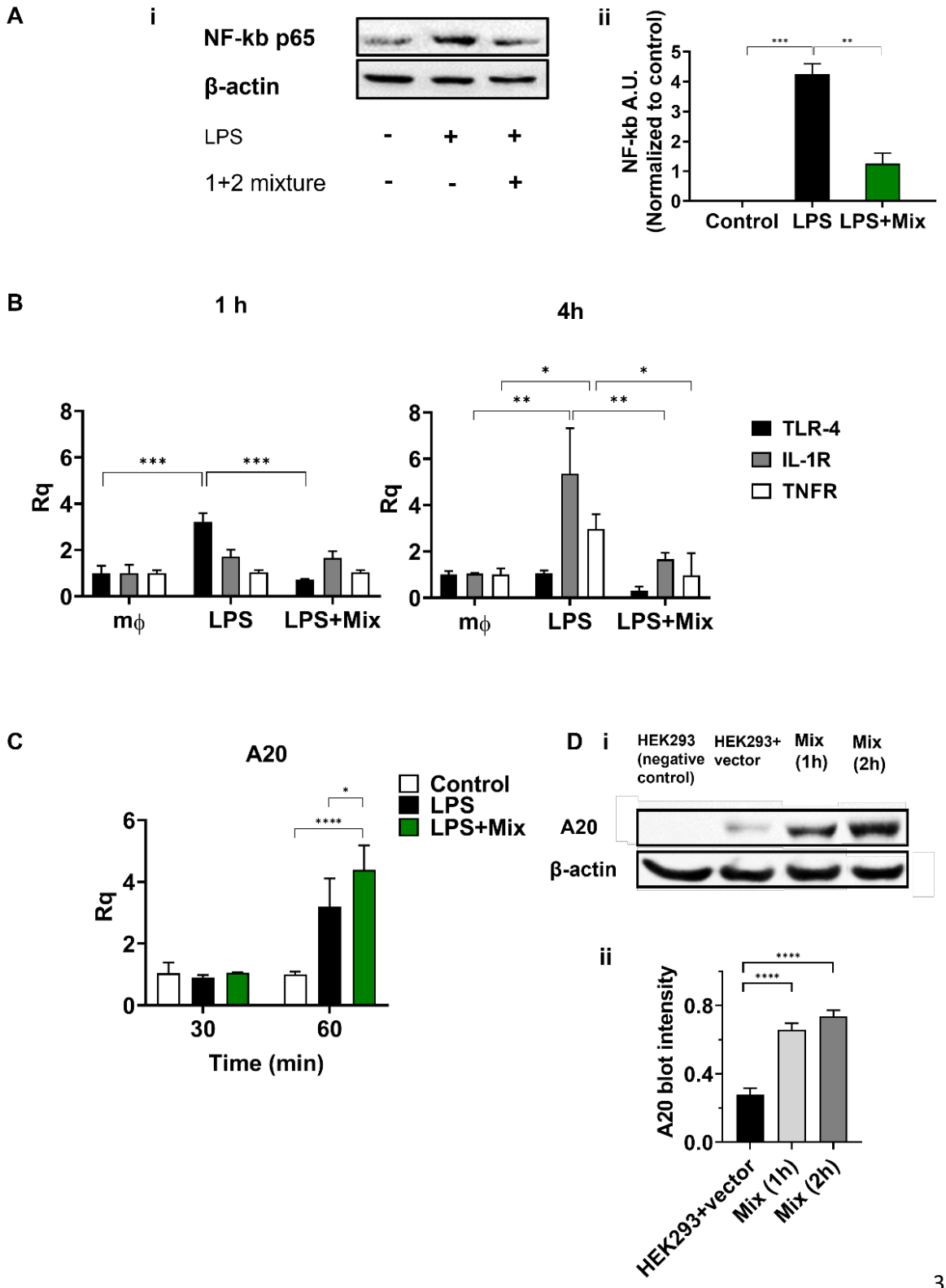

Figure 6. Molecular mechanisms underlining the anti-inflammatory activity of the tryptophol acetate and tyrosol acetate mixture. Intraperitoneal macrophages were obtained 72 hours after thioglycolate injection and cultured with LPS with or without **1+2** mixture. (**A**) At different time intervals, cell lysates were assessed by Western blot (WB). (**i**) Representative WB of phosphorylated NF-κB (p65) protein expression, with the effects of the mixture (100 μM each). (**ii**) Relative band intensity histograms. The

graph represents an average of three independent experiments. Bars indicate standard errors of the means; **p<0.001, ***p<0.0001. Beta-actin was used to assess equal protein loading. (**B**) RAW 264.7 cell line was used for definition of the NF-kB pathway related receptors. Cells were incubated with LPS with and without molecules at the indicated time intervals. RNA was extracted and cDNA was analyzed by RT-PCR. (**C**) Relative protein and mRNA expression of A20 after stimulation with 1 μg/ml of LPS in the absence and presence of **1**+**2** mixture (100μM), detected by RT-qPCR. Error bars indicate standard deviations of three independent cultures. * P<0.05, **** P< 0.0001 ANOVA followed by Tukey's post hoc analysis. (**D**) (**i**) HEK-293T cells were transfected with pCAGGA vector (*HA-A20*) (1.5 μg) and incubated with and without **1+2** mixture (1 or 2 h). Protein expression of A20 in cell lysates is presented in WB. HEK-293T cells were used as a negative control. (**ii**) Relative band intensity histograms. The graph represents an average of three independent experiments. Bars indicate standard error of the means; statistical analysis calculated by Unpaired t-test, p<0.0001. Beta-actin was used to ascertain equal protein loadings.

To shed further light on the parameters responsible for NF-κB attenuation incurred by tryptophol acetate and tyrosol acetate in LPS-stimulated macrophages, we evaluated expression of prominent upstream receptors associated with NF-κB cascades, specifically TLR4, IL-1R and TNFR [39] (Figure 6B). The bar diagrams in Figure 6B depicts the levels of the receptors' mRNA recorded in RAW 264.7 macrophage cells, stimulated by LPS in the presence or absence of **1** + **2** mixture. Figure 6B demonstrates that addition of the molecules to the LPS-stimulated cells significantly attenuated expression of the genes of all three receptors. Specifically, LPS stimulation induced expression of *TLR4* during the first hour (black bar, Figure 6B, left), while co-addition of **1**+**2** mixture together with LPS resulted in suppression of *TLR4* expression, reverting to the baseline (pre-inflammation) level. Similarly, tryptophol acetate and tyrosol acetate significantly attenuated expression of both *IL-1R* (grey bars) and *TNFR* (white bars) 4 hours after LPS stimulation, giving rise to baseline expression levels in both receptors.

Accounting for the reduction of the upstream receptors in the NF-κB pathways by the tryptophol acetate and tyrosol acetate (e.g., Figure 6B), we further tested the effects of the molecules upon expression of the A20 protein, known to suppress signaling cascades associated with the TLR receptors [40] (Figure 6C-D). The bar diagram in Figure 6C presents experimental data corresponding to RAW 264.7 cells treated with **1+2** mixture and the A20 m-RNA levels measured after 30 min and 60 min. As shown in Figure 6C, both LPS, and the **1+2** mixture co-added with LPS, induced significant expression of A20 gene within 60 minutes after addition to the cells. However, when **1+2** were co-added to the cells together with LPS, significantly higher expression of A20 was found.

To assess the protein level of A20, we further carried out WB analysis (Figure 6D), employing HEK-293T cells transfected with the pCAGGA mammalian expression vector (HA-A20), allowing transient transfection of A20 [41,42]. Specifically, after transfection, the tryptophol acetate and tyrosol acetate mixture was incubated with the cells for different time intervals (HEK-293T cells were used as a negative control, Figure 6D,i). The WB data in Figure 6D demonstrate that **1+2** mixture induced significant expression of A20, both after 1 and 2 h of incubation compared to the control HEK-293T cells comprising the vector. Together, the RT-PCR and WB results in Figure 6C-D suggest that modulation of A20 levels by tryptophol acetate and tyrosol acetate is likely a key factor in attenuation NF-κB expression and concomitant anti-inflammatory effects of the molecules.

Tryptophol acetate and tyrosol acetate affect mouse gut microbiome

In tandem with elucidating the dramatic clinical effects and molecular facets of the inflammation modulatory activities of tryptophol acetate and tyrosol acetate, we also examined the effect of the molecules on gut microbiome of the mice (Figure 7). The relationship between gut microbiota and host immune properties has recently emerged as a prominent factor in systemic response to inflammation. Previous seminal studies, for example, linked inflammatory cytokine production and individual variations in cytokine response to the composition and function of the microbiota [43]. In the experiments depicted in Figure 7, mice microbiome analysis was carried out through collecting the stool samples from all participating mice, the day before and at intervals of 6 h and 24 h after LPS injection. The microbial taxonomic 16S rRNA gene sequences were subsequently determined.

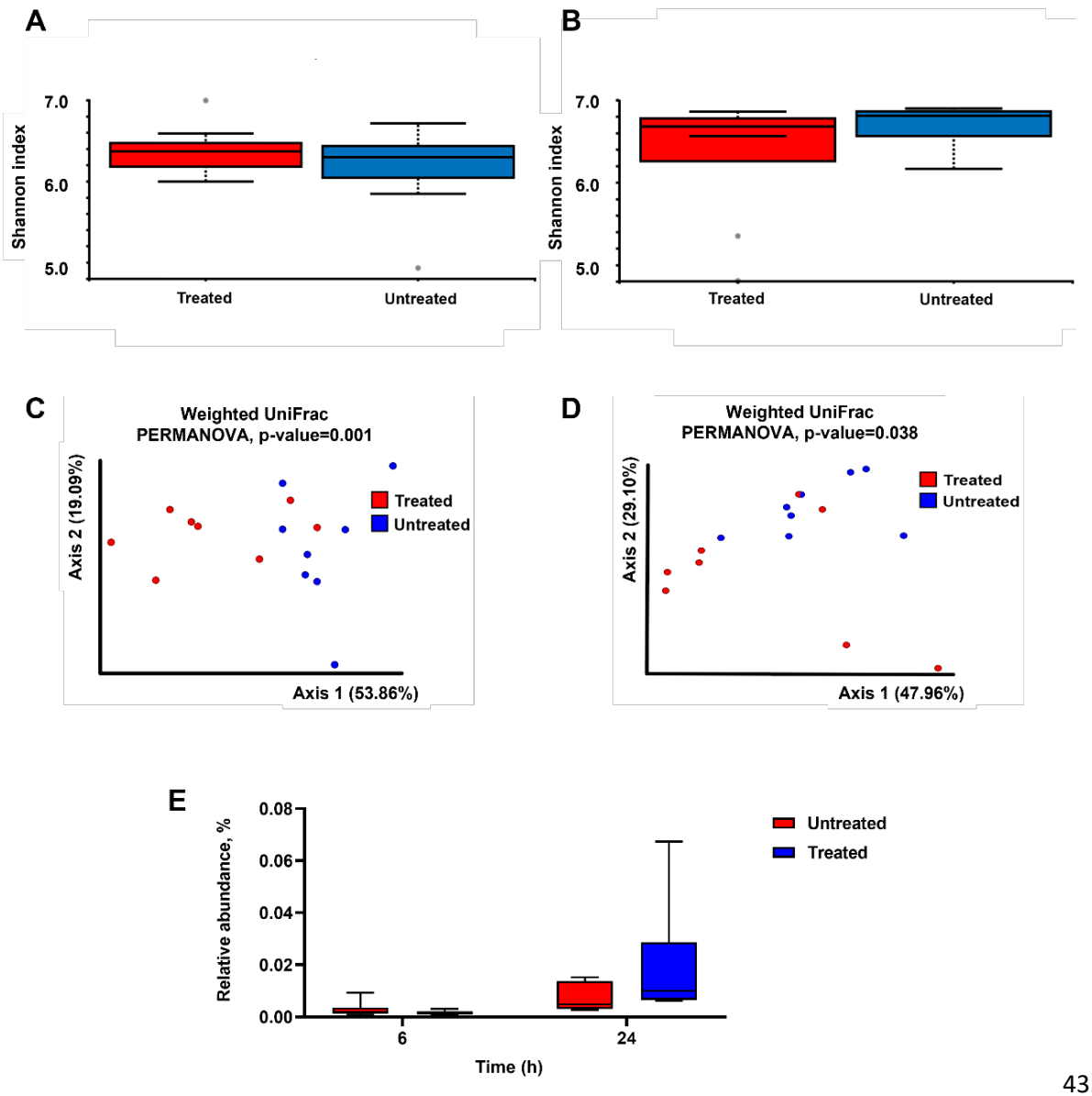

Figure 7. Effect of tryptophol acetate and tyrosol acetate mixture treatment on mice microbiome. (A, B) Alpha diversity analysis using the Shannon index after (**A**) 6 hours (p=0.46) and (**B**) 24 hours of treatment (p=0.29); quantitative variables were compared between groups with the Wilcoxon U-test, for non-normally distributed data. **(C, D)** Principal coordinate analysis plot representing beta-diversity based on weighted UniFrac distances after **(C)** 6 hours (permutational multivariate analysis of variance, P=0.001) and **(D)** 24 hours of treatment (permutational multivariate analysis of variance, P=0.038). (**E**) Bacterial taxa *Bacteroides ovatus* relative abundance (%) boxplots for untreated and molecules treated groups. The taxa more abundant in treated group 24 h from LPS injection. (Treated and untreated, n=8)

When comparing the microbial richness (i.e., alpha diversity; Figure 7A, B) before and after treatment with tryptophol acetate and tyrosol acetate (at 6 hours and 24 hours,

respectively), no significant differences were observed (Wilcoxon test, P=0.46 and P=0.29). However, we found differences in beta diversity (i.e., between sample diversities; Figure 7C, D) between treated and untreated mice 6 and 24 hours after LPS injection (PERMANOVA, P=0.001 and P=0.038, respectively). This important observation indicates that although the species richness was not significantly altered between the treated and untreated mice, dysbiosis (shift in the microbiome) at the community level was already observed 6 hours after LPS administration. Dysbiosis 6 hours after LPS treatment was characterized by a profound reduction in the relative abundance of commensals such as *Blautia*, *Bacteroides*, *Clostridium, Sutterella* and *Parabacteroides* and by an increase in the relative abundance of *Ruminococcus* (Table S1, Supporting information). These changes occurred in both the treated and untreated groups. Twenty-four hours after LPS administration we observed a decrease in the relative abundance of *Blautia, Bacteroides, Clostridium and Oscillospira* and increase in the relative abundance of *Ruminococcus*.

Figure 7E underscores the effect of treating the LPS-administered mice with tryptophol acetate and tyrosol acetate. Importantly, the abundance of *Bacteroides* increased in the mice that were treated with **1+2** compared to the mice that were not treated (24 hours after LPS injection; Figure 7E). This taxon was also abundant in the microbiome of healthy mice (ANCOM test significance W=68 and W=72 respectively (Table S1)). This result is important as *Bacteroides* has been linked to varied immune-protective and anti-pathogenic activities associated with microbiome modifications [44].

Discussion

Current therapy of sepsis is mainly based on anti-bacterial and symptomatic treatments. Important strategies for overcoming sepsis syndromes have been based on blocking cytokines and other pro-inflammatory molecules. While mortality from sepsis significantly decreased in the past century, in many cases of septic shock or cytokine storms, for example associated with the recent SARS-Covid-19 pandemic, mortality is high [2,9]. In most patients experiencing such sepsis syndromes, various inflammatory factors are responsible for the development of multiorgan failure and new therapeutic approaches which target upstream pro-inflammatory molecules are highly sought.

In this work, we identified two metabolites secreted by the probiotic fungus *Kluyveromyces marxianus* in a milk-fermented microorganism mixture (kefir) – tryptophol acetate and tyrosol acetate - which exhibit remarkable anti-inflammatory activities. Comprehensive *in vivo, ex vivo* and *in vitro* experiments demonstrate an effective blocking of the "cytokine storm" by an equimolar mixture of the two molecules. Specifically, we observed that mice inflicted with LPS-induced sepsis and orally treated with tryptophol acetate and tyrosol acetate, had significantly milder patterns of the disease in comparison with LPS-administrated control mice that received only buffer. Importantly, no mice mortality was observed both upon co-administration of the molecules with LPS (i.e., sepsis preventive effect), as well as upon providing the molecules to mice already displaying signs of severe inflammation (Figure 2).

LPS administration in mice yields clinical signs of human sepsis. Thus, we assessed the effects of tryptophol acetate and tyrosol acetate mixture on systemic inflammation and on various vital organs in LPS-injected mice (Figures 3-5). In sepsis, multiorgan destruction due to severe inflammation leads to hepatic and renal failure,

respiratory distress, dysfunction of gastrointestinal system and hematological changes, such as coagulation disorders [45]. The reported experimental data demonstrate that orally administered tryptophol acetate and tyrosol acetate mixture prevented tissue damage and attenuated hematological changes. Specifically, the molecules' mixture attenuated alveolar wall degradation, and in parallel decreased lung congestion (Figure 3A). Tryptophol acetate and tyrosol acetate also significantly affected recruitment of myeloid cells, which are intimately involved in exacerbation of lung inflammation [46]. Indeed, we observed that mixture of tryptophol acetate and tyrosol acetate reduced recruitment of neutrophils and Ly6C-positive monocytes into lungs (Figure 3A, iii). Moreover, histology analyses reveal that, after treatment with the molecules, more abundant mature F4/80-positive macrophages was detected, likely accounting for tissue repair [29,34] (Figure 3A, iii). We also recorded substantial healing effects in the case of LPS-induced liver tissue damage, in which the molecules stemmed the loss of hepatic cells (Figure 3B), and reduced crypt damage in intestinal tissue (Figure 3C).

The systemic therapeutic effects of tryptophol acetate and tyrosol acetate were further analyzed *in vivo* and *ex vivo* (Figure 4). We found that LPS-administered mice treated with the molecules' mixture displayed lower anemia and thrombocytopenia that usually accompany severe septic syndromes and cytokine storms (Figure 4A). Furthermore, significant reduction in the expression of pro-inflammatory cytokines in lung tissue and in serum were recorded after treating LPS-injected mice with the tryptophol acetate and tyrosol acetate mixture (Figure 4B and 4C). These results are significant, since release of pro-inflammatory mediators, including cytokines, chemokines and ROS is the hallmark of cytokine storms [47].

Particularly significant in this context were the *in vivo* and *in vitro* data recorded for IL-6, specifically the attenuation of this pro-inflammatory cytokine by orders of

magnitude to the baseline level after treatment with tryptophol acetate and tyrosol acetate (Figure 4B, 4C; Figure 5B). Cytokine storm syndromes in COVID-19 patients, for example, have been associated with dramatic increase in blood IL-6 levels, and IL-6 concentrations have been shown as markers for fatality outcomes [48]. As such, the considerable and rapid reduction of IL-6 levels induced by the tryptophol acetate and tyrosol acetate point to potential therapeutic avenue for severe inflammation syndromes, such as affected by COVID-19. Additional *ex vivo* experiments in Figure 5D assessing pro-inflammatory cytokine secretion echoed the *in vivo* results, demonstrating attenuated secretion of pro-inflammatory cytokines by LPS-stimulated macrophages in the presence of the tryptophol acetate and tyrosol acetate mixture. Importantly, different from numerous anti-inflammatory strategies reported in the literature and clinically employed, tryptophol acetate and tyrosol acetate did not induce complete immunosuppression, rather the molecules reverted the pro-inflammatory cytokine levels to baseline (pre-inflammation) values.

A major question underlying the anti-inflammatory effects of tryptophol acetate and tyrosol acetate concerns their mode of action. *Ex vivo* experiments utilizing LPS-stimulated murine peritoneal macrophages reveal important mechanistic aspects (Figures 5-6). Specifically, in parallel with inhibition of pro-inflammatory cytokines, we recorded a significant reduction in ROS levels. ROS include short-lived bioactive molecules produced by immune competent cells serving as messenger molecules for various physiologic and pathologic processes [49]. ROS particularly activate multiple inflammatory signaling pathways [50]. Notably, we recorded a significant reduction in ROS levels after tryptophol acetate and tyrosol acetate were added to LPS-activated murine peritoneal macrophages (Figure 5A). It should be noted that while tryptophol acetate and tyrosol acetate significantly attenuated the pathophysiological

consequences of severe inflammation, the molecules did not adversely affect core immune processes, particularly phagocytosis activity (Figure 5B-C). These results are consistent with previous studies, reporting anti-inflammatory and anti-oxidant effects without impairing macrophage bactericidal activities [51,52].

To account for the broad-based immune modulation effect of tryptophol acetate and tyrosol acetate, particularly the significant reduction in pro-inflammatory cytokine levels, we investigated the impact of the molecules' mixture upon the immune signaling pathway involving NF-κB (Figure 6). NF-κB is central to transcription pathways of many genes encoding pro-inflammatory mediators and plays a crucial role in varied inflammatory disease conditions [37]. Indeed, addition of tryptophol acetate and tyrosol acetate reduced NF-κB level in macrophages stimulated with LPS (Figure 6A). Furthermore, the RT-PCR data in Figure 6 attest to pronounced downregulation of the main upstream receptors involved in NF-κB activation - TLR4, IL-1R and TNFR. These observations are mechanistically significant as it is known that production and secretion of pro-inflammatory cytokines are governed by the TLR/NF-κB signaling pathway, perceived as a major "gateway" cascade in innate immunity, and are associated with the pathogenesis of severe inflammation that promotes lung, liver, and intestinal injuries[44]. For example, binding of LPS to TLR-4 was shown to induce lung parenchymal damage, neutrophil accumulation in the interstitial and alveolar compartments, elevated vascular permeability and pulmonary edema [53,54].

Further molecular insight upon the underlying immunomodulatory mechanism of tryptophol acetate and tyrosol acetate was furnished by analysis of A20 protein levels (Figure 6). A20 is a prominent negative feedback regulator of NF-κB signaling. It has been reported that mice genetically deficient in A20 develop severe inflammation, underscoring the central role of A20 in suppression of NF-kB-dependent inflammation

and tissue homeostasis [55]. Importantly, we found that the tryptophol acetate and tyrosol acetate mixtures significantly induced, in both gene and protein levels, the expression A20 (Figure 6 C,D). Thus, our data suggest that the protection furnished against severe inflammation by tryptophol acetate and tyrosol acetate may be mediated by triggering A20 expression and concomitant inhibition of the TLR4/IL-1R/TNFR-NF-κB pathway.

Due to our observations that administration of tryptophol acetate and tyrosol acetate orally gave rise to the pronounced anti-inflammatory effects, we assessed the effects of the molecules on the gut microbiota (Figure 7). The relationship between severe inflammation and microbial dysbiosis has been extensively studied in recent years [56,57]. The gut microbiota have been shown to enhance host immunity to pathogens, and dysbiosis has been linked to increased susceptibility of severe inflammation [58]. Accordingly, we characterized the gut microbial compositions of mice prior and after LPS injection, and with / without treatment with the mixture of tryptophol acetate and tyrosol acetate. Indeed, oral administration of the molecules had a significant impact on the community composition, manifested by an increase in the abundance of bacteria with anti-inflammatory properties [59]. Notably, the predominant change recorded was the increase in the genus *Bacteroides* in mice that were treated with the molecules 24 hours after LPS administration (Figure 7E).

Recent studies have reported on the anti-inflammatory properties of *Bacteroides* [60]. The mechanisms of action proposed for these anti-inflammatory activities include inhibition of pathogen colonization [44] and increased mucosal barrier by modifying goblet cells and mucin glycosylation [61]. The higher abundance of *Bacteroides* upon treating the LPS-injected mice with tryptophol acetate and tyrosol acetate may thus account to “cross-talk” between the molecules and host microbiota, promoting intestinal homeostasis. Moreover, the significance of these results are further

underlined by a recent study stressing the need for substances that protect gut microbiota such as *Bacteroides* from the collateral damage of widely used antibiotics such as tetracyclines and macrolides [62]. Thereby, consumption of tryptophol acetate and tyrosol acetate in combination with antibiotics may present a new approach for reducing the harmful side effects of antibiotics on host gut microbiome.

Overall, varied food-extracted substances have been touted as exhibiting powerful antioxidant and anti-inflammatory properties [63]. However, reports presenting comprehensive clinical, physiological, and mechanistic analyses of the anti-inflammatory activities of probiotic yeast secreted metabolites, such as presented here for tryptophol acetate and tyrosol acetate, have been rare. In particular, to the best of our knowledge, no previous studies have shown an exceptional clinical outcome (i.e. survival and morbidity results, Figure 2), combined with a comprehensive mechanistic analysis. Indeed, our findings uncover, in detail, the immune pathways underlying anti-inflammatory effects of probiotic-sourced molecules.

In conclusion, we discovered that metabolites secreted by a probiotic yeast abundant in a milk-fermented microorganism mixture – tryptophol acetate and tyrosol acetate –significantly inhibit systemic severe inflammation effects. Comprehensive *in vivo, ex-vivo,* and *in vitro* data demonstrate the healing and protective effects of the two molecules, including prevention of mortality in mice experiencing LPS-induced severe inflammation, blocking organ damage, reduction of ROS production, and maintaining healthy peripheral blood cell profile. Particularly important, the experiments demonstrate that, unlike many anti-inflammatory treatments, tryptophol acetate and tyrosol acetate did not induce immunosuppression, but rather effectively restored baseline levels of pro-inflammatory cytokines and inhibited activation of NF-κB through elevating A20 expression. Overall, the remarkable systemic anti-inflammatory

effects of tryptophol acetate and tyrosol acetate and their presence in a food source that has been consumed by humankind for millennia may open new avenues for anti-inflammatory therapeutics.

Materials and Methods

Materials

Dulbecco's Modified Eagle Medium (DMEM), Roswell Park Memorial Institute (RPMI 1640), heat-inactivated fetal bovine serum (FBS) were purchased from Biological Industries (Beit Haemek, Israel). Penicillin, streptomycin, ECL western blotting substrate, opti-MEM, and Bradford reagent were purchased from Thermo-fisher. Dihydrochloride (AAPH), 2,2-Diphenyl-1-picrylhydrazyl (DPPH), 2,20 –azobis (2-amidinopropane, fluorescein, hydrogen peroxide, sodium citrate, acetonitrile, formic acid, sulfuric acid, ethanol, methanol, sodium carbonate, lipopolysaccharide (from E. coli O55:B5, L2880), propidium iodide (PI) (Solution P4864), NaCl, Triton X-100, BSA, NaF, Na_3VO_4, AEBSF, polyethylenemine (PEI), Leupeptin, and Aprotinin were purchased from Sigma-Aldrich. Xylene was purchased from Epredia (lot 6601). Tris buffer was purchased from Bio-lab (Jerusalem, Israel). Thioglycolate was purchased from life technologies, 2085262 (ultra-pure grade). All reagents and solvents were of analytical grade and were used as received.

DPPH scavenging activity

The effect of tryptophol and tyrosol acetates on DPPH• radical were estimated according to recommendations of Marinova and Batchvarov [24] with some modifications. All of the solutions were prepared in ethanol. The stock solution was prepared by dissolving 13.8 mg DPPH with 20 mL ethanol and stored until needed. The

control (100%) solution was obtained by mixing 225 µL ethanol with 25 µL stock solution to obtain an absorbance of 1.0 ± 0.1 units at 490 nm. 200 µL of tryptophol acetate and tyrosol acetate dissolved in ethanol in a concentration of 200 µM was allowed to react with 25 µL of the DPPH solution for 20 min in the dark at 400 rpm at 25ºC. Ethanol (250 µL) was used for the blank control (100%), and 225 µL was used as a blank. The absorbance decrease was recorded at 490 nm. For all evaluated assays, absorbance measurements were performed in triplicate using a Microtiter Plate Reader (Varioskan Flash, Thermo) to calculate radical scavenging activity (% of inhibition) with the formula.

$$\text{Inhibition (\%)} = 1 - \frac{\text{Abs (sample)} - \text{Abs (blank)}}{\text{Abs (control)} - \text{Abs (blank)}} \times 100$$

where Abs (sample) was the absorbance of the reaction in the presence of the sample (sample dilution + DPPH solution), Abs (blank) was the absorbance of the blank for each sample dilution (sample dilution + DPPH solvent), and Abs (control) was the absorbance of the control reaction (sample solvent + DPPH solution).

Oxygen radical absorbance capacity (ORAC assay)

The ORAC method is based on the oxidative degradation of the fluorescent molecules after mixing with a free radical generator, for example, azo compounds. This method determines the ability of the sample to neutralize short-lived free radicals. The assay was carried out according to Ou et al. [25], with some minor modifications. Prior to the measurements, tryptophol acetate and tyrosol acetate were dissolved in acidified methanol to a concentration of 200 µM. 30 µL of each molecule or 30 µL mixture of both, as well as blank (methanol) were mixed with 180 µL of 112 nM fluorescein solution in a 96-well plate and incubated at 37°C for 15 min. Subsequently, 100 µL of

100 mM 2,2' -azobis(2-amidinopropane) dihydrochloride (AAPH) solution was added, and the fluorescence was measured every 70 s for 90 min using a Microtiter Plate Reader (Varioskan Flash, Thermo). The excitation wavelength was 485 nm and the emission recorded at 520 nm. All stock solutions and dilutions of samples were prepared fresh daily in phosphate-buffered saline (PBS, pH 7.4). The experiments were done in six repetitions. Results are presented according to the following calculations :

Area under the curve (AUC) was calculated for each sample using the equation:

$AUC = 1 + FU_1/FU_0 + FU_2/FU_0 + FU_3/FU_0 \ldots\ldots +$

FU_0 = fluorescence at time zero.

FU_x = fluorescence at specific timepoints (e.g., FU_3 is the fluorescence value at three minutes). Net AUC was calculated by subtracting the Blank AUC from the AUC of each sample using the equation:

Net AUC = AUC (Antioxidant) – AUC (blank)

Animal studies

C57BL/6 mice

All experiments were performed in accordance with the Institutional Animal Care and Use Committee at Ben-Gurion University (IL-43-07-2020). Eight-week-old C57BL/6 mice (Harlen, Rehovot, Israel) weighing approximately 20 gr were held in specific pathogen-free conditions at the University Central Research Facility for at least one week prior to commencing studies. The mice were fed (*ad libitum*) with V1154-703 ssniff™ (Soest, Germany) and were allowed water continuously. Environmental enrichment was provided to all animals based on the requirements of the particular mouse strain. Temperature was maintained at 21°C, and animals were exposed to a 12

h light, 12 h dark cycle with a 15 min ramp-up and ramp-down to simulate dusk and dawn. The mice were divided into two study groups: untreated (mice injected with LPS and administered a placebo), Treated (mice injected with LPS and treated by oral administration of mixture of tryptophol acetate and tyrosol acetate). Mice were housed in groups of six per cage. LPS dose was 30 mg/kg to each mouse (~20 g), which was injected intraperitoneally.

Treatment with tryptophol acetate and tyrosol acetate

Tryptophol acetate and tyrosol acetate were synthesized as previously described [22] and dissolved in DDW to desired concentrations (final concentration of 150 µg/kg). The molecular mixture was administrated through oral gavage in a volume of 200 µL twice per day, in the morning (08:30–09:30) and evening (19:30–20:30). DDW was used as a placebo and was administrated orally to the control group at the same times.

In one set of experiments, the mixture of molecules was administrated concomitantly with LPS injection and treatment was continued two times per day until the end time of the experiment (156 h). In another set of experiments, the first treatment with the molecules started 28 h after LPS injection and was continued two times per day until the end time of the experiment (156 h).

Clinical evaluation of inflammation

Clinical signs of inflammation were recorded twice daily. Measurement of body weight, signs of diarrhea and appearance of blood traces in stool, as well as signs of dyspnea were assessed. Mean percentage of weight loss was calculated daily as the ratio of measured body weight and weight measured before injection of LPS. Every 6 h after LPS injection till endpoint of the experiments (till 72 h), mice were anesthetized with 5% isoflurane (2-chloro-2-(difluoromethoxy)-1,1,1-trifluoro-ethane) and blood

samples were got from tail vien. Lungs, livers, colons, and intestinals were obtained at the same time intervals and were cleaned from contents by flushing with 10 ml of sterile PBS. The tissue were taken for extraction of RNA and part of them were embedded in paraffin following a standard protocol. 5-µm sections using a rotary microtome (MRC-Lab, HIS-202A). Paraffin embedded tissues were cut into 5-µm sections using a rotary microtome (MRC-Lab, HIS-202A), rehydrated and stained with hematoxylin.

Immunohistochemistry Staining

Tissue sections were de-paraffinized in xylene and re-hydrated with decreasing concentrations of alcohol. Subsequently, endogenous peroxide was blocked with hydrogen peroxide, and antigen retrieval was achieved by treating sections with 0.01M sodium citrate, pH 6.0 for 1 min in a pressure cooker. After blocking with universal blocking solution (ZYMED Laboratories, San Francisco, CA), tissue sections were stained with the designated primary antibodies. A Vectastain Elite ABC Peroxidase kit or Universal ImmPRESS kit (Vector Laboratories, Burlingame, CA) were used for secondary antibodies, and visualization was performed using 3-amino-9-ethylcarbazole (AEC) as a substrate (ZYMED Laboratories, San Francisco, CA). Sections were then stained with hematoxylin for counterstaining and mounted using VectaMount AQ Aqueous Mounting Medium (Cat-No. H-5501; Vector Laboratories). Myeloperoxidase (MPO)-positive (Abcam), F4/80-positive (Santa Cruz, 377009), and LY6C-positive cells (Abcam, ab15627) were counted in stained sections in six randomly chosen fields (×200), and bars are indicated standard errors of the means.

Blood count

Blood samples were collected from mice tails with EDTA micropipette capillaries (Exigo) and analyzed directly after collection by a veterinary hematology analyzer (Exigo H400, Boule Medical AB, Spånga, Sweden).

Cytokine measurements by ELISA

To measure the extent of the inflammatory response in mice, serum obtained from the blood of LPS-treated and untreated mice, we customized a highly sensitive milliplex® MAP Kit (Cat # MPXMCYTO-70K; Millipore) with color-coded beads and fluorescent dyes according to the manufacturer's recommendations.

***In vitro* macrophage experiments**

264.7 cell line

The RAW 264.7 cell lines (third passage) were purchased from American Type Culture Collection (ATCC1 TIB-71™). Cells were cultured in DMEM with 10% FBS and 1% penicillin/streptomycin, in an atmosphere of 5% CO2 and 95% humidity at 37°C. Cells were regularly tested for mycoplasma contamination.

Peritoneal macrophages

Mouse peritoneal macrophages were obtained from C57BL/6J mice (6–8weeks old) 72 hours after intra-peritoneum injection of Thioglycolate and cultured in complete RPMI medium with and without LPS (100ng/ml) (O55:B5, L2880, Sigma) and in the presence or absence of the tryptophol acetate and tyrosol acetate (1+2 mixture).

Cytokine production in peritoneal macrophages 760

Cells (3×10^5) were seeded in 24-well plates and after 24 h, supernatants were collected 761
and assessed for cytokine secretion. To measure the extent of the inflammatory 762
response in the LPS stimulated peritoneal macrophages, we used murine ELISA kits 763
according to the manufacturers' recommendations for IL-1β (PeproTech,, 900-K47), 764
IL-6 (Biotest, DY406), TNF-α (Biotest, DY410), TGF-β (Biotest, DY1679), IL-1α 765
(Biotest, MAB400-500; AB-monoclonal BAF400, AB-polyclonal 400-ML-005), and 766
INF-β (BioLegend B292426). 767

ROS analysis 768

Peritoneal macrophage cells were seeded (1×10^5 cells) into 96-well plates for ROS and 769
phagocytosis analysis. 770

After 2 h of incubation in complete medium at 37°C, cells were stimulated with LPS 771
(100ng\ml) and incubated overnight in the absence or presence of tryptophol acetate 772
and tyrosol acetate (100 μM each). After 24 hours, the cells were washed two times 773
with PBS and incubated for 1 h with CellROX Deep Red Reagent (Invitrogen, Carlsbad, 774
CA) prior to analysis by flow cytometry. Dead cells were gated out using PI. The 775
presence of ROS was analyzed by the fluorescence geometric mean (GM) of the 776
CellROX Deep Red fluorescence. 777

Phagocytosis analysis 778

Peritoneal macrophage cells were seeded in 96-well plates with RPMI medium. After 779
2 adherences at 37°C, all the cells were stimulated with LPS (100ng\ml) and incubated 780
overnight in the absence or presence of the tryptophol acetate and cytosol acetate 781
mixture (100 μM each). After 24 hours the cells were washed two times with PBS and 782

incubated for 1 h or 3 h at 37°C in 200 µl RPMI medium, alone (control) or with Fluoresbrite® Yellow-Green carboxylate microspheres (1 µm) (Polysciences Inc., 15702) in a ratio of 3:1 beads-to-cells. In the flow cytometry analysis, dead cells were gated out using PI. Free beads were analyzed alone and gated out from the analysis. The fraction of live cells positive for beads was used to estimate phagocytosis functionality.

Western blot analysis for NF-κB expression

Protein expression was monitored using Western blot analysis. $10x10^6$ murine peritoneal macrophages were seeded on petri dishes. After overnight incubation at 37°C the cells were stimulated with LPS (100ng/ml) in the absence or presence of the mixture of tryptophol acetate and tyrosol acetate (100 µM each molecule) and incubated for 30 minutes and harvested in lysis buffer (50 mL 3M NaCl, 25 mL 1M Tris pH 7.5, 10 mL Triton X-100, and 10 mL 0.5M EDTA were mixed and added to 905 mL distilled water) in the presence of protease inhibitor cocktail (1:50 complete, Sigma-Aldrich, Israel). Lysates were placed on ice for 30 min and then centrifuged for 30 min (12,000 rpm) at 4°C. Supernatants (cytosolic fractions) were collected, and protein concentrations were determined using a Bio-Rad protein assay kit (lot 5000202, Israel). SDS sample buffer was added, and samples were boiled for 5 min and then frozen at -20°C until use. NF-κB (after 30 minutes) was assayed using cell lysates (70µg), separated on SDS-PAGE and analyzed using the following: antibody raised against the anti-NF-κB (p-65) (1:1000; abcam, ab32536), β-actin (1:1000; MP Biomedicals, Santa Ana, CA).

Real-time PCR

Total mRNA from obtained tissues and RAW 264.7 macrophages was extracted using a RNA extraction kit (ISOLET II RNA Mini Kit, Bioline). cDNA was synthesized from

1 µg of RNA using a PrimeScriptTM RT reagent kit (Lifegene, Bio-52073). Subsequent real-time PCR was performed with an iCycler iQ™ Real-Time PCR Detection System (Bio-RAD). PCR results were analyzed with SDS 2.02 software (Applied Biosystems, Thermo). The level of target gene expression was calculated following normalization of the GAPDH gene level in each sample and presented as relative units. Quantitative PCR was performed with Taqman Master Mix (Rhenium, Israel) for: TLR4 (Cat 4453320, Assay ID Mm00445273_m1), Tnfrsf1b (Cat 4453320, Assay ID Mm00441889_m1), GAPDH (Cat 4453320, Assay ID Mm99999915_g1), and IL-1R (Cat 4453320, Assay ID Mm00434237_m1) or with Mix SYBR Green Master Mix (Applied Biosystems).

Gene	**Forward sequences (5′–3′)**	**Reverse sequences (5′–3′)**
IL-1α	GTTACAGTGAAACGAAGACTAC	TGCAAGTCTCATGAAGTGAGC
IL-6	TTCCTCTCTGCAAGAGACTTC	GTTGGGAGTGGTATCCTCTGT
IL-1β	TGCCACCTTTTGACAGTGATG	TGTGCTGCTGCGAGATTTGA
HPRT	AGTCCCAGCGTCGTGATTAG	TGGCCTCCCATCTCCTTCAT

Table 1. Primers used for RT-qPCR of target gene

A20 expression in HEK-293 T cells

Cells: HEK-293 T cells were grown and maintained in Dulbecco's Modified Eagle's Medium (DMEM) at 37 °C and 5% CO_2, supplemented with 10% fetal calf serum and antibiotics (50 units/ml penicillin, 50 µg/ml streptomycin).

Antibodies and plasmids 825

Mouse monoclonal antibodies (mAbs) specific for A20 (Santa Cruz Biotechnology, 826
Inc., Santa Cruz, CA). Mouse anti-β-actin mAbs (Merck Millipore, Darmstadt, 827
Germany). Horseradish peroxidase (HRP)-conjugated goat anti-mouse Abs (Abcam 828
Biotechnology). The full-length human or mouse A20 cDNA with a human influenza 829
hemagglutinin (HA) tag cloned in a pCAGGA mammalian expression vector (HA-A20) 830
was kindly provided by Dr. Shai Cohen (Cancer and Vascular Biology Research Center, 831
The Rappaport Faculty of Medicine and Research Institute, Technion, Israel), 832
previously described [42] . 833

Transient transfection in HEK-293 T cells 834

HEK-293 T cells were chosen for transient plasmid transfection. Briefly, 5 x 10^5 HEK- 835
293 T cells were plated and left to grow for 24 hours in the incubator (37 °C and 5% 836
CO_2). The following day, old DMEM medium was replaced with serum free-fresh 837
DMEM and the cells were left in the incubator for 30 minutes. DNA (plasmids) samples 838
were prepared for transfection; 1.5 µg of purified HA-A20 plasmid DNA was added to 839
250 µL of Opti-MEM medium, then 5 µL of (final concentration of 5 µg/mL) of 840
polyethylenimine (PEI) was added to the DNA, vortexed and incubated at RT for 20 841
minutes. The PEI-DNA mix was, added to the cells steadily drop by drop and the cells 842
were left in the incubator (37 °C and 5% CO_2) for 4 hours. After the transfection, the 843
cells were incubated with the Molecule mix (200 µM each) for time range of 1 and 2 h. 844
Cells were harvested at indicated time points and lysed in lysis buffer containing 25mM 845
Tris HCl, pH 7.5, 150mM NaCl, 5mM EDTA, 1mM Na_3VO_4, 50mM NaF, 10µg/ml 846
each of leupeptin and aprotinin, 2mM AEBSF and 1% Triton X-100) followed by 30 847
min incubation on ice. Lysates were centrifuged at 13,000 rpm for 30 min at 4°C and 848

the nuclear-free supernatants were used further analysis. 20 µg of protein was resolved on 10% SDS-PAGE and blotted on to nitrocellulose membrane. Membranes were immunoblotted with mouse anti-A20 (1:2000) and mouse anti-β-actin mAbs (1:500) as indicated and visualized following ECL exposure.

Protein concentration

Protein concentration was measured by the method of Bradford using bovine serum albumin as standard.

Electrophoresis and immunoblotting

Whole cell lysates were resolved by electrophoresis on 10 % polyacrylamide gels using Bio-Rad Mini-PROTEAN II cells. Gel proteins were electroblotted onto nitrocellulose membranes (Schleicher and Schuell) at 100 V for 1 h, using BioRad Mini Trans-Blot transfer cells. After 1 h of membrane blocking with 3% BSA in TBS at 37 °C, the membranes were incubated with the indicated primary Abs followed by extensive washings in TBST and incubation with HRP-conjugated goat anti-mouse. Immunoreactive protein bands were visualized using the enhanced chemiluminescent.

Data analysis

All results are expressed as the mean ± SD or mean ±SE, as indicated. Data for all in-vivo and in-vitro experiments were analyzed by a one/two-way ANOVA followed by Tukey post-hoc test using GraphPad Prism (GraphPad Software, San Diego, Ca). A p-value of ≤ 0.05 was considered statistically significant.

Fecal microbiome analysis

Total DNA was extracted from fecal samples using a PureLink microbiome DNA extraction kit (Invitrogen, Carlsbad, CA) followed by a 2-min bead-beating step, as previously described by Shouval, R. et al. [64]. Purified DNA was PCR amplified using PrimeSTAR Max (Takara-Clontech, Shiga, Japan) for the variable V4 region (using 515F-806R barcoded primers) of the 16S rRNA gene. Amplicons were purified using Agencourt AMPure XP magnetic beads (Beckman-Coulter, Brea, CA), and subsequently quantified using a Quant-It Picogreen dsDNA quantitation kit (Invitrogen, Carlsbad, CA). Equimolar DNA amounts from individual samples were pooled and sequenced using the Illumina MiSeq platform at the Genomic Center, Azrieli Faculty of Medicine, Bar-Ilan University, Israel. Sequencing data were processed using QIIME2 version 2019.10. [65]. Single end sequences with a similarity ≥ 99% were assigned as the same feature. Taxonomy was assigned using the GreenGenes database [66]. Chimeric sequences were removed with DADA2 (--p-trunc-len 160) [67]. Samples with <1000 features and features with total frequency <2 were filtered out. Rarefaction was done using 5,000 sequences per sample. Alpha and beta diversity were calculated based on rarefied datasets.

Statistical analysis of microbiome results

The distribution pattern of quantitative variables was examined using a Shapiro-Wilk test. Quantitative variables were compared between groups with a Wilcoxon U-test, for non-normally distributed data, respectively. All tests were 2-tailed, and in all, $p \leq 0.05$ was considered significant . Bacterial alpha diversity was assessed by the Shannon index. Statistical significance of microbial alpha diversity differences was confirmed using a Kruskal–Wallis test, followed by paired Mann-Whitney tests, with Benjamini-

Hochberg correction for the false discovery rate. Beta diversity was calculated using weighted UniFrac distances. Statistical significance was confirmed using a permutational multivariate analysis of variance (PERMANOVA). Differences in relative abundances of bacterial taxa between groups were identified using the ANCOM method [65].

Acknowledgements

We thank Dr Shai Cohen (Cancer and Vascular Biology Research Center, The Rappaport Faculty of Medicine and Research Institute, Technion - Israel) for providing the A20-plasmid, and his help with the A20 experiments.

Author contributions

Conceived and designed the experiments O.M., R.M, E.V. and R.J.; experiments and data analysis O.M., R.M., M.B., M.K., J.S., E.T., E.S., and B.R.; writing—original draft O.M., R.M., E.V. and R.J.; writing - reviewed and edited the manuscript B.R., O.K., and E.V.; All authors read and approved the final manuscript.

Disclosures

A company - Biotic Therapeutics - has been co-founded by O.M. and R.J. based on this research.

References

1. Chen, L. *et al.* Inflammatory responses and inflammation-associated diseases in organs. *Oncotarget* **9**, 7204–7218 (2018).
2. Moriyama, K. & Nishida, O. Targeting cytokines, pathogen-associated molecular patterns, and damage-associated molecular patterns in sepsis via blood purification. *Int. J. Mol. Sci.* **22**, (2021).
3. Akira, S. & Hemmi, H. Recognition of pathogen-associated molecular patterns by TLR family. *Immunol. Lett.* **85**, 85–95 (2003).
4. Costa, R. T. *et al.* T helper type cytokines in sepsis: time-shared variance and

correlation with organ dysfunction and hospital mortality. *Brazilian J. Infect. Dis.* **23**, 79–85 (2019).

5. Melo, A. K. G. *et al.* Biomarkers of cytokine storm as red flags for severe and fatal COVID-19 cases: A living systematic review and meta-analysis. *PLoS One* **16**, 1–21 (2021).
6. Hotchkiss, R. S. *et al.* Sepsis and septic shock Richard. *Physiol. Behav.* **176**, 139–148 (2017).
7. Furman, D. *et al.* Chronic inflammation in the etiology of disease across the life span. *Nat. Med.* **25**, 1822–1832 (2019).
8. Huang, Q. *et al.* Targeting inflammation and cytokine storm in COVID-19. *Pharmacol. Res.* **159**, 105051 (2020).
9. Yang, L. *et al.* The signal pathways and treatment of cytokine storm in COVID-19. *Signal Transduct. Target. Ther.* **6**, 1–20 (2021).
10. Niva, M. 'All foods affect health': Understandings of functional foods and healthy eating among health-oriented Finns. *Appetite* **48**, 384–393 (2007).
11. Dirienzo, D. B. Effect of probiotics on biomarkers of cardiovascular disease: Implications for heart-healthy diets. *Nutr. Rev.* **72**, 18–29 (2014).
12. Luna, R. A. & Foster, J. A. Gut brain axis: Diet microbiota interactions and implications for modulation of anxiety and depression. *Curr. Opin. Biotechnol.* **32**, 35–41 (2015).
13. Hewlings, S. J. & Kalman, D. S. Curcumin: A review of its effects on human health. *Foods* **6**, 1–11 (2017).
14. Meng, X., Zhou, J., Zhao, C. N., Gan, R. Y. & Li, H. Bin. Health benefits and molecular mechanisms of resveratrol: A narrative review. *Foods* **9**, 1–27 (2020).
15. Proestos, C. The Benefits of Plant Extracts for Human Health. *Foods* **9**, 1653 (2020).
16. Giada, M. de L. R. Food Phenolic Compounds: Main Classes, Sources and Their Antioxidant Power, Oxidative Stress and Chronic Degenerative Diseases - A Role for Antioxidants. *Oxidative Stress Chronic Degener. Dis. - A Role Antioxidants* 87–112 (2013).
17. Mennen, L. I., Walker, R., Bennetau-Pelissero, C. & Scalbert, A. Risks and safety of polyphenol consumption. *Am. J. Clin. Nutr.* **81**, 326–329 (2005).
18. Franco, M. C. *et al.* Administration of kefir-fermented milk protects mice against Giardia intestinalis infection. *J. Med. Microbiol.* **62**, 1815–1822 (2013).
19. Vinderola, C. G. *et al.* Immunomodulating capacity of kefir. *J. Dairy Res.* **72**, 195–202 (2005).
20. Malka, O. *et al.* Cross-kingdom inhibition of bacterial virulence and communication by probiotic yeast metabolites. *Microbiome* **9**, 1–15 (2021).
21. Rothschild, D. E., McDaniel, D. K., Ringel-Scaia, V. M. & Allen, I. C. Modulating inflammation through the negative regulation of NF-κB signaling. *J. Leukoc. Biol.* **103**, 1131–1150 (2018).
22. Jelinek R, Malka O, Kalson D, Meijler MM, K. A. Microorganism mixtures, Molecules Derived Therefrom, and Methods of Use Thereof WO 2020/031191. (2020).
23. Bardaweel, S. K. *et al.* Reactive oxygen species: The dual role in physiological and pathological conditions of the human body. *Eurasian J. Med.* **50**, 193–201 (2018).
24. Marinova, G. & Batchvarov, V. methods DPPH. *Bulg. J. Agric. Sci.* **17**, 11–24 (2011).
25. Ou, B., Hampsch-Woodill, M. & Prior, R. L. Development and validation of an improved oxygen radical absorbance capacity assay using fluorescein as the fluorescent probe. *J. Agric. Food Chem.* **49**, 4619–4626 (2001).
26. Anderberg, S. B., Luther, T. & Frithiof, R. Physiological aspects of Toll-like receptor 4 activation in sepsis-induced acute kidney injury. *Acta Physiol.* **219**, 575–590 (2017).
27. Parker, S. J. & Watkins, P. E. Experimental models of Gram-negative sepsis. 22–30 (2001).
28. Shimabukuro-Vornhagen, A. *et al.* Cytokine release syndrome. *J. Immunother. Cancer* **6**, (2018).

29. Arora, M., Poe, S. L., Ray, A. & Ray, P. LPS-induced CD11b+Gr1intF4/80+ regulatory myeloid cells suppress allergen-induced airway inflammation. *Int. Immunopharmacol.* **11**, 827–832 (2011).
30. Hirata, F. *et al.* Insulin enhances leukocyte-endothelial cell adhesion in the retinal microcirculation through surface expression of intercellular adhesion molecule-1. *Microvasc. Res.* **69**, 135–141 (2005).
31. Abraham, E. Neutrophils and acute lung injury. *Crit. Care Med.* **31**, 1–5 (2003).
32. O'Dea, K. P. *et al.* Mobilization and Margination of Bone Marrow Gr-1 high Monocytes during Subclinical Endotoxemia Predisposes the Lungs toward Acute Injury . *J. Immunol.* **182**, 1155–1166 (2009).
33. O'Dea, K. P. *et al.* Lung-marginated monocytes modulate pulmonary microvascular injury during early endotoxemia. *Am. J. Respir. Crit. Care Med.* **172**, 1119–1127 (2005).
34. Uderhardt, S. *et al.* 12/15-Lipoxygenase Orchestrates the Clearance of Apoptotic Cells and Maintains Immunologic Tolerance. *Immunity* **36**, 834–846 (2012).
35. Jabbour, H. N., Sales, K. J., Catalano, R. D. & Norman, J. E. Inflammatory pathways in female reproductive health and disease. *Reproduction* **138**, 903–919 (2009).
36. Grivennikov, S. I., Greten, F. R. & Karin, M. Immunity, Inflammation, and Cancer. *Cell* **140**, 883–899 (2010).
37. Mittal, M., Siddiqui, M. R., Tran, K., Reddy, S. P. & Malik, A. B. Reactive oxygen species in inflammation and tissue injury. *Antioxidants Redox Signal.* **20**, 1126–1167 (2014).
38. Oeckinghaus, A. and & Ghosh, S. The nuclear factor- k B (NF-k B) family of transcription factors. *Cold Spring Harb. Perspect. Biol.* **1**, 1–15 (2009).
39. Verstrepen, L. *et al.* TLR-4, IL-1R and TNF-R signaling to NF-κB: Variations on a common theme. *Cell. Mol. Life Sci.* **65**, 2964–2978 (2008).
40. Kawai, T. & Akira, S. The role of pattern-recognition receptors in innate immunity: Update on toll-like receptors. *Nat. Immunol.* **11**, 373–384 (2010).
41. Hitoshi, N., Ken-ichi, Y. & Jun-ichi, M. Efficient selection for high-expression transfectants with a novel eukaryotic vector. *Gene* **108**, 193–199 (1991).
42. Lapid, D., Lahav-Baratz, S. & Cohen, S. A20 inhibits both the degradation and limited processing of the NF-κB p105 precursor: A novel additional layer to its regulator role. *Biochem. Biophys. Res. Commun.* **493**, 52–57 (2017).
43. Schirmer, M. *et al.* Linking the Human Gut Microbiome to Inflammatory Cytokine Production Capacity. *Cell* **167**, 1125-1136.e8 (2016).
44. Hiippala, K. *et al.* Isolation of anti-inflammatory and epithelium reinforcing bacteroides and parabacteroides spp. From a healthy fecal donor. *Nutrients* **12**, (2020).
45. Huang, M., Cai, S. & Su, J. The pathogenesis of sepsis and potential therapeutic targets. *Int. J. Mol. Sci.* **20**, (2019).
46. Rosseau, S. *et al.* Phenotypic characterization of alveolar monocyte recruitment in acute respiratory distress syndrome. *Am. J. Physiol. - Lung Cell. Mol. Physiol.* **279**, 25–35 (2000).
47. Kumar, V. Toll-like receptors in sepsis-associated cytokine storm and their endogenous negative regulators as future immunomodulatory targets. *Int. Immunopharmacol.* **89**, 107087 (2020).
48. Huang, L. *et al.* Sepsis-associated severe interleukin-6 storm in critical coronavirus disease 2019. *Cell. Mol. Immunol.* **17**, 1092–1094 (2020).
49. Reczek, C. R. & Chandel, N. S. ROS-dependent signal transduction. *Curr. Opin. Cell Biol.* **33**, 8–13 (2015).
50. Forrester, S. J., Kikuchi, D. S., Hernandes, M. S., Xu, Q. & Griendling, K. K. Reactive oxygen species in metabolic and inflammatory signaling. *Circ. Res.* **122**, 877–902 (2018).
51. Hidalgo H., Humberto A., Helmke R., German V. The effect of cyclosporine and dexamethasone on an alveolar macrophage cell line (NR8383). *Transplantation* **53**, 620–623 (1992).

52. Pooladanda, V. *et al.* Nimbolide protects against endotoxin-induced acute respiratory distress syndrome by inhibiting TNF-α mediated NF-κB and HDAC-3 nuclear translocation. *Cell Death Dis.* **10**, (2019).
53. Jeyaseelan, S., Chu, H. W., Young, S. K., Freeman, M. W. & Worthen, G. S. Distinct roles of pattern recognition receptors CD14 and Toll-like receptor 4 in acute lung injury. *Infect. Immun.* **73**, 1754–1763 (2005).
54. Zanoni, I. *et al.* CD14 controls the LPS-induced endocytosis of toll-like receptor 4. *Cell* **147**, 868–880 (2011).
55. Lee, E. G. *et al.* Failure to regulate TNF-induced NF-kappaB and cell death responses in A20-deficient mice. *Science* **289**, 2350–4 (2000).
56. Hakansson, A. & Molin, G. Gut microbiota and inflammation. *Nutrients* **3**, 637–687 (2011).
57. Wang, J., Chen, W. D. & Wang, Y. D. The Relationship Between Gut Microbiota and Inflammatory Diseases: The Role of Macrophages. *Front. Microbiol.* **11**, 1–9 (2020).
58. Belkaid, Y. and T. H. Role of the Microbiota in Immunity and inflammation Yasmine. *Cell* **157**, 121–141 (2015).
59. Krasulova, K. & Illes, P. Intestinal interplay of quorum sensing molecules and human receptors. *Biochimie* **189**, 108–119 (2021).
60. Delday, M., Mulder, I., Logan, E. T. & Grant, G. Bacteroides thetaiotaomicron Ameliorates Colon Inflammation in Preclinical Models of Crohn's Disease. *Inflamm. Bowel Dis.* **25**, 85–96 (2019).
61. Wrzosek, L. *et al.* Bacteroides thetaiotaomicron and Faecalibacterium prausnitziiinfluence the production of mucus glycans and the development of goblet cells in the colonic epithelium of a gnotobiotic model rodent. *BMC Biol.* **11**, 61 (2013).
62. Maier, L. *et al.* Unravelling the collateral damage of antibiotics on gut bacteria. *Nature* **599**, 120–124 (2021).
63. Bakasatae, N., Kunworarath, N., Takahashi Yupanqui, C., Voravuthikunchai, S. P. & Joycharat, N. Bioactive components, antioxidant, and anti-inflammatory activities of the wood of Albizia myriophylla. *Rev. Bras. Farmacogn.* **28**, 444–450 (2018).
64. Shouval, R. *et al.* Patterns of salivary microbiota injury and oral mucositis in recipients of allogeneic hematopoietic stem cell transplantation. *Blood Adv.* **4**, 2912–2917 (2020).
65. Bolyen, E. *et al.* Reproducible, interactive, scalable and extensible microbiome data science using QIIME 2. *Nat. Biotechnol.* **37**, 852–857 (2019).
66. DeSantis, T. Z. *et al.* Greengenes, a chimera-checked 16S rRNA gene database and workbench compatible with ARB. *Appl. Environ. Microbiol.* **72**, 5069–5072 (2006).
67. Callahan, B. J. *et al.* DADA2: High-resolution sample inference from Illumina amplicon data. *Nat. Methods* **13**, 581–583 (2016).

Supporting information

Tryptophol acetate and tyrosol acetate, metabolites secreted by a probiotic yeast, display remarkable anti-inflammatory effects

ANCOM results after 6 hours			
ASVs	**Healthy**	**Untreated**	**Treated**
Blautia	High	Low	Low
Bacteroides	High	Low	**Low**
Clostridium	High	Low	Low
Sutterella	High	Low	Low
Ruminococcus	Low	High	High
Parabacteroides	High	Low	Low

ANCOM results after 24 hours			
ASVs	**Healthy**	**Untreated**	**Treated**
Blautia	High	Low	Low
Bacteroides	High	Low	**High**
Clostridium	High	Low	Low
Oscillospira	Low	High	High
Ruminococcus	Low	High	High

Table 1 ANCOM results of mice treated and untreated with molecules. Main bacterial taxa abundance after 6 and 24 hours from LPS administration.